Modeling and Simulation of Polypropylene Particle Size Distribution in Industrial Horizontal Stirred Bed Reactors

Zhou Tian,[1] Xue-Ping Gu,[1] Lian-Fang Feng,[1] Jean-Pierre Corriou,[2] Guo-Hua Hu[2]

[1]*State Key Laboratory of Chemical Engineering, Department of Chemical and Biological Engineering, Zhejiang University, Hangzhou, Zhejiang 310027, People's Republic of China*
[2]*Laboratory of Reactions and Process Engineering, CNRS-Nancy University, ENSIC-INPL, 1 rue Grandville, BP 20451, Nancy 54001, France*

Received 2 February 2011; accepted 9 November 2011
DOI 10.1002/app.36473
Published online 30 January 2012 in Wiley Online Library (wileyonlinelibrary.com).

ABSTRACT: This work aims at developing a steady-state particle size distribution (PSD) model for predicting the size distribution of polypropylene particles in the outflow streams of propylene gas-phase horizontal stirred bed reactors (HSBR), on the one hand and investigating the effect of the catalyst residence time distribution (RTD) on the polymer PSD, on the other hand. The polymer multilayer model (PMLM) is used to describe the growth of a single particle. Knowing the PSD and RTD of a Ziegler–Natta type of catalyst and polymerization kinetics, this model allows calculating the polymer PSD of propylene polymerization in the HSBRs. The calculated polypropylene PSDs agree well with those obtained from the industrial reactors. The results reveal that both the PSD and the RTD of the catalyst affect the polymer PSD but in different manners. The effect of RTD on the PSD is less significant in the case of a nonuniform size catalyst feed. This model also allows investigating the effects of other process parameters on the polymer PSD under steady-state conditions, including intraparticle mass- and heat-transfer limitations, initial catalyst size, and polymer crystallinity. © 2012 Wiley Periodicals, Inc. J Appl Polym Sci 125: 2668–2679, 2012

Key words: particle size distribution; modeling; residence time distribution; horizontal stirred bed reactor; polypropylene

INTRODUCTION

Catalyst systems mostly used in recent years for polypropylene production are the higher generation Ziegler–Natta catalysts. They are supported systems in the form of porous pellets. Polymerization proceeds, as the monomer transfers from the gas phase or the liquid phase to active sites. The formation of polymer particles replicates catalyst particles whose diameters usually range from 10 to 200 μm. The diameters of the ultimate polymer particles usually range from 100 to 5000 μm.[1,2] Particle size distribution (PSD) is a very important morphological characteristic of polypropylene particles.[3,4] On the other hand, it may not only influence the hydrodynamics of a fluidized bed reactor (FBR) but also have a significant effect on the elastomer content in the case of high-impact polypropylene.[5]

Many efforts are made to account for the polymer PSD in olefin polymerization reactors. Table I provides a concise overview on some of the works on the subject. It shows that the PSD models proposed in the literature are mainly focused on gas-phase FBRs. Population balance models (PBMs) are often developed to investigate the PSD in olefin polymerization reactors.

However, only a limited amount of work has been devoted to the horizontal stirred bed reactor (HSBR), which cannot be considered as a single continuous stirred tank reactor (CSTR) due to its characteristic configuration.[13,14] The literature regarding the effect of residence time distribution (RTD) on the polymer PSD is also relatively scarce. Dittrich and Mutsers[11] proposed a modeling approach describing the RTD in a HSBR and simulated the PSD with different RTD models. For simplicity, the intraparticle mass- and heat-transfer resistances were not considered in their work. Moreover, most of the PSD models in the literature are not validated with any industrial scale data. Nevertheless, it is very useful to refer to them when developing new PSD models. The work reported in this article aims at developing a steady-state PSD model coupled with a single particle growth model for predicting the size of polypropylene particles in the outflow streams of HSBRs. It is validated by data generated in industrial reactors.

Correspondence to: X.-P. Gu (guxueping@zju.edu.cn) or G.-H. Hu (guo-hua.hu@ensic.inpl-nancy.fr).

Contract grant sponsor: National Basic Research Program of China; contract grant number: 2009cb320603.
Contract grant sponsor: State Key Laboratory of Chemical Engineering; contract grant number: SKL-ChE-08D03.

TABLE I
A Brief Summary of Studies on the PSD in Polyolefin Reactors

Authors	System[a]	Reactors	Model	Remark
Choi et al.[6]	PE	FBR	PBM	Steady state; perfectly back-mixed reactor;
Soares and Hamielec[7]	–	CSTR	–	Steady state; effect of reactor RTD on polymer PSD;
Zacca[2]	PP	VSBR, HSBR, FBR, and loop reactors	PBM	Steady state; catalyst residence time as main coordinate;
Hatzantonis et al.[8]	PE	FBR	PBM	Steady state; perfectly back-mixed reactor; inclusion of particle attrition and agglomeration effects;
Yiannoulakis et al.[9]	E–P	FBR	PBM	Steady state; perfectly back-mixed reactor; incorporation of PFM model and PBM; inclusion of particle agglomeration effects;
Kim and Choi[10]	E–P	FBR	PBM	Steady state; multicompartment model; inclusion of particle segregation;
Harshe et al.[3]	PP	FBR	PBM	Prediction of polymer properties;
Dompazi et al.[4]	E–P	FBR	PBM	Dynamic; multiscale, multiphase, multizone; prediction of particle segregation;
Dittrich and Mutsers[11]	PP	HSBR	–	Steady state; incorporation of RTD and backmixing in the HSBR;
Luo et al.[12]	PP	Tubular loop reactor	PBM	Steady state; effects of process parameters on PSD;

[a] PE: polyethylene; PP: polypropylene; E–P: ethylene–propylene copolymer.

The effects of the intraparticle mass and heat limitations on the particle growth rate and the final polymer PSD are investigated. The effect of the catalyst RTD on the polymer PSD is also simulated for both uniform and nonuniform catalyst size feeds.

PROCESS DESCRIPTION

Figure 1 is a scheme of the gas-phase polypropylene process using HSBRs in series. Unlike slurry and solution processes, no liquid phase but vapor and solids are present in the HSBRs. In the first HSBR, the catalyst, usually a fourth-generation Ziegler–Natta catalyst with titanium as the active component, is fed to the front end of the reactor where it reacts with the monomers in the gas phase. The reaction heat is removed by spraying condensed monomers at various locations along the top of the reactor. The reactor is horizontally placed and cylindrical in shape, and it contains several zones that are sometimes separated by weirs. It involves mechanical agitation, rather than fluidization. Paddles connected to a rotating shaft mildly agitate the polymer powder. The reacting powder moves slowly toward the reactor outlet from which it is discharged. The agitation provides a typical axial powder mixing pattern which is unique for polyolefin gas-phase reactors. Hence, the HSBR cannot be considered as a single CSTR due to its characteristic configuration,[2,15,16] as will be discussed in detail in the following section. Table II shows the operating conditions for the HSBRs.

MATHEMATICAL MODELS

Modeling of RTD

The RTD of a single CSTR cannot correctly describe that of a HSBR. Caracotsios found that the flow in a HSBR behaved, as though it was moving through three to five equivolume CSTRs in series.[13] Other authors also used the concept of equivolume CSTRs in series for describing a HSBR.[2,16] More recently, Dittrich and Mutsers[11] proposed a semimechanistic model to take into account mixing and mass transfer. They recommended not using flow models with a lumped parameter for backmixing but describing axial net transport and backmixing separately then superimposing them for flow modeling. They compared four flow models for a HSBR. Models 1 and 2 were cascades of CSTRs of equal residence times (Model 1) or equal volumes (Model 2) with a simple overflow from one CSTR to the next. The RTD for those two models are described by eqs. (1) and (2), respectively.[2,15,17]

$$E(t) = \frac{t^{N_{CSTR}-1}}{\tau_i^{N_{CSTR}}(N_{CSTR}-1)!} e^{-t/\tau_i} \quad (1)$$

$$E(t) = \sum_{i=1}^{N_{CSTR}} \frac{\tau_i^{N_{CSTR}-2}}{\Pi_{j=1,j\neq i}^{N_{CSTR}}(\tau_i - \tau_j)} \exp\left(\frac{-t}{\tau_i}\right) \quad (2)$$

where N_{CSTR}, the number of CSTRs, is the parameter for the RTD model.

TABLE II
Operating Conditions for the Propylene Gas-Phase HSBRs

Reactors	R1	R2
Temperature (°C)	70	66
Pressure (bar)	21.2	22.1
Volume (m^3)	92	92
Mean residence time (h)	2.32	1.4

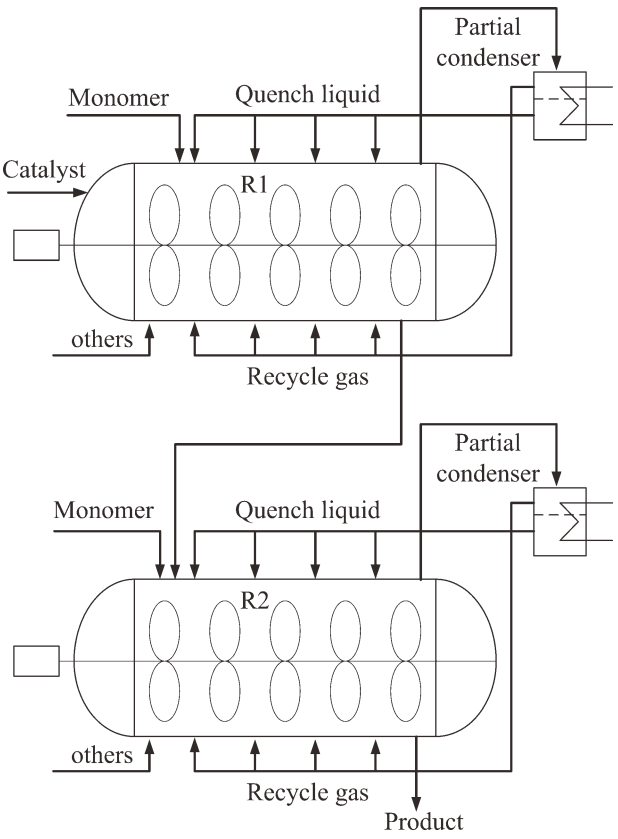

Figure 1 Gas-phase polypropylene process using HSBR in series.

Models 3 and 4 were backflow models that reflected the outcome of the tracer experiments. In this work, Models 1–3 are used for describing or predicting the RTD. Moreover, the spline function is used to treat Dittrich's RTD data (Model 3).[18] The resulting RTD function is incorporated in a PSD model developed in this work.

Modeling of a single particle growth

The literature used the so-called polymer multilayer model (PMLM) to simulate the growth of a single polymer particle.[19–21] The model assumes that growing polymer chains and catalyst fragments form a continuum. A schematic representation of the PMLM is shown in Figure 2. The whole particle is divided into concentric spherical layers as in the multigrain model,[22] but microparticles are not considered. At the beginning of the polymerization, the active sites are distributed uniformly inside all layers. The monomer concentration and temperature are calculated at the boundaries of each layer using a three-point Lagrangian interpolation polynomial. The average concentrations of the monomer in the layers are used to calculate the polymerization rate of the layers in each time interval. According to the amount of polymer formed in that time interval, the volume of each layer is updated. The monomer and temperature profiles are recalculated for the new boundary positions, and the process is repeated for the next time interval. It should be pointed out that the boundary conditions of the model used here are somewhat different from those of the PMLM.[19,21] Ranz–Marshall correlations, which are often used in gas-phase catalytic olefin polymerization,[23–25] are applied to this study to calculate the gas–solid film mass- and heat-transfer coefficients for growing polymer particles. The PMLM accounting for the intraparticle mass- and heat-transfer limitations comprises the following differential equations and boundary conditions:

$$\frac{\partial M}{\partial t} = \frac{1}{r^2}\frac{\partial}{\partial r}\left(D_{\text{eff}} r^2 \frac{\partial M}{\partial r}\right) - R_M \tag{3}$$

$$\frac{\partial T}{\partial t} = \frac{1}{\rho_p C_p}\frac{1}{r^2}\frac{\partial}{\partial r}\left(k_e r^2 \frac{\partial T}{\partial r}\right) + \frac{(-\Delta H_r)}{\rho_p C_p} R_M \tag{4}$$

where M is the propylene concentration in the polymer particle, T, the temperature in the polymer particle, D_{eff}, the effective monomer diffusion coefficient, R_M, the propylene consumption rate (mol/m^3 s), k_e, the thermal conductivity of the polymer, and $-\Delta H_r$ the polymerization heat. Equations (3) and (4) are subjected to following initial and boundary conditions:

Initial conditions

$$t = 0, \qquad M = 0; \quad T = T_{\text{bulk}} \tag{5}$$

Boundary conditions

$$r = 0, \qquad \frac{\partial M}{\partial r} = \frac{\partial T}{\partial r} = 0 \tag{6}$$

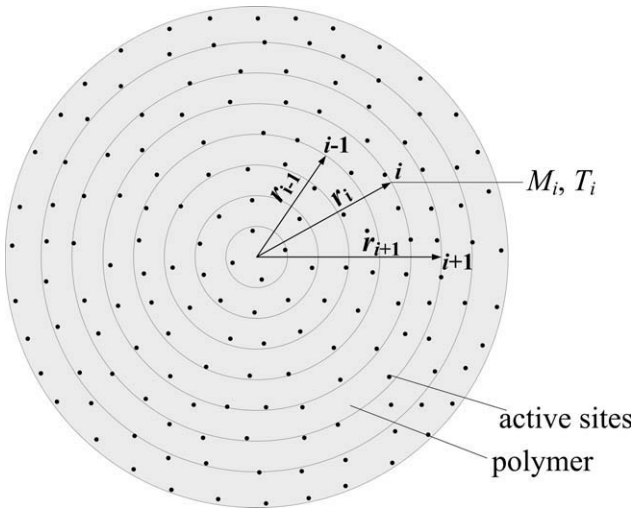

Figure 2 A schematic representation of the PMLM.

$$r = R, \quad -D_{\text{eff}}\frac{\partial M}{\partial r} = h_m(M - M_{\text{bulk}}); \quad -k_e\frac{\partial T}{\partial r} = h(T - T_{\text{bulk}}) \tag{7}$$

where M_{bulk} and T_{bulk} are the monomer concentration and temperature of the bulk phase (gas phase herein), respectively. h_m and h are the external gas–solid film mass-transfer and heat-transfer coefficient, respectively. The values of h_m and h are given by the well-known Ranz–Marshall correlations as follows:

$$\text{Sh} = 2 + 0.6\text{Sc}^{1/3}\text{Re}^{0.5} \tag{8}$$

$$\text{Nu} = 2 + 0.6\text{Pr}^{1/3}\text{Re}^{0.5} \tag{9}$$

where $\text{Sh} = h_m d_p/D_{\text{bulk}}$, $\text{Sc} = \mu_g/\rho_g D_{\text{bulk}}$, $\text{Re} = d_p u_r \rho_g/\mu_g$, $\text{Nu} = d_p h/\lambda_g$, and $\text{Pr} = \mu_g C_{pg}/\lambda_g$ are the dimensionless Sherwood, Scmidt, Reynolds, Nusselt, and Prandtl numbers, respectively.

The volume and boundary position of each layer must be updated after a prescribed time interval Δt. The monomer concentrations in the previous time step are used for this purpose, and the equations are expressed as

$$V_i^1 = \frac{4}{3}\pi\left[\left(r_i^1\right)^3 - \left(r_{i-1}^1\right)^3\right] \tag{10}$$

$$V_i^j = V_i^{j-1}\left[1 + \frac{k_{p_i}^j C_i^{*j-1} C_{m_i}^j M_w\left(t_j - t_{j-1}\right)}{\rho_p}\right] \tag{11}$$

$$r_{i+1}^j = \left[\frac{3}{4\pi}V_{i+1}^j + \left(r_i^j\right)^3\right]^{1/3} \tag{12}$$

In these equations, the superscripts and subscripts indicate the time and radial position, respectively. For example, V_i^j and r_i^j are the volume of layer i and its radial position in the polymer particle at the jth time interval, respectively. To update the volume, the concentration of active sites that depends on the volume of layers in layer i at the jth time interval, C_i^{*j}, is expressed as

$$C_i^{*j} = C_i^{*j-1} V_i^{j-1}/V_i^j \tag{13}$$

The radial profiles of the monomer concentration, the temperature, and the active sites inside the polymer particle are obtained from the PMLM. Moreover, the particle growth rate $G(D)$, which links the single particle growth with the polymer PSD model, can also be determined from the PMLM. The cubic spline method is used to fit the particle growth rate with D as an independent variable and G as a dependent one. Then $G(D)$ is incorporated in the PSD model to predict the distribution of the polymer particle size.

TABLE III
Kinetic Scheme of Propylene Homopolymerization over a Ziegler–Natta Catalyst

Activation	$S_p \xrightarrow{k_f} C^*$
Chain propagation	$C^* - P_j + M \xrightarrow{k_p} C^* - P_{j+1}$
Deactivation	$C^* \xrightarrow{k_d} C_d + D_j$

Polymerization kinetics

The literature on the kinetics of Ziegler–Natta catalyzed polymerization of propylene is abundant.[26–29] This type of catalyst tends to produce polymers with a broad molecular weight distribution because of the nature of the multiple active sites. However, the particle growth rate depends mainly on the elementary reactions of chain activation, propagation, and deactivation. The effect of the chain transfer to hydrogen and monomer on the polymer particle size could be neglected. Therefore, a single active site kinetic model, which composes of chain activation, propagation, and deactivation, is used to calculate polymer particle growth rate, as shown in Table III.

1. Consumption of the potential catalyst:

$$\frac{dS_p}{dt} = -k_f S_p \tag{14}$$

2. Activation reaction of the potential catalyst:

$$\frac{dC^*}{dt} = k_f S_p - k_d C^* \tag{15}$$

3. Accumulation of the dead catalyst:

$$\frac{dC_d}{dt} = k_d C^* \tag{16}$$

4. Propagation of the polymer chains at the active catalytic site:

$$R_p = k_p\ C^*\ C_m \tag{17}$$

The polymerization rate can be calculated by integrating eqs. (14)–(17) and is expressed by eq. (18)[30]:

$$R_p = k_p\ C_m\ k_f\ C_0^*[\exp(-k_f t) - \exp(-k_d t)]/(k_d - k_f) \tag{18}$$

with

$$k_f = k_{f0}\ \exp(E_{\text{af}}/R_{\text{gas}}T) \tag{19}$$

$$k_p = k_{p0}\ \exp(E_{\text{ap}}/R_{\text{gas}}T) \tag{20}$$

$$k_d = k_{d0}\ \exp(-E_{\text{ad}}/R_{\text{gas}}T) \tag{21}$$

where k_f is the activation rate constant, E_{af}, the activation energy for the lumped activation reaction, k_p,

the propagation rate constant, E_{ap}, the activation energy for the lumped propagation reaction, T, the temperature, C_m, the concentration of monomer absorbed in the polymer and can be calculated according to the procedure described in the subsequent section monomer sorption effect, C_0^*, the initial concentration of active centers (mol/kg-cat), k_d, the deactivation constant, and E_{ad}, the activation energy for the lumped deactivation reaction. The kinetic scheme incorporated in the model is purposely kept as simple, as it can describe the catalyst activity profile and predict the polymer growth rate sufficiently well.

Effect of the monomer sorption

The effect of the monomer sorption is an important aspect, because it dictates the actual monomer concentration C_m in the polymer. In semicrystalline polymers, sorption occurs only in the amorphous polymer phase. The actual monomer concentration depends on the crystallinity of the polymer according to the equation[31]

$$C_m = a_\varphi [M]^* \tag{22}$$

where $[M]^*$ is the moles of the penetrant per unit volume amorphous polymer. The amorphous volume fraction, a_φ, can be determined from the polymer density, according to the relation

$$a_\varphi = \frac{\rho_c - \rho_p}{\rho_c - \rho_a} \tag{23}$$

where ρ_c and ρ_a are the densities of crystalline and amorphous polymers, respectively. Henry's law can be applied for the sorption of relatively light propylene in polypropylene under gas-phase conditions.

$$[M]^* = k^* P_m \tag{24}$$

where k^* is the Henry constant and P_m, the monomer pressure. The value of the Henry constant can be calculated from the following equation[31,32]:

$$\log(k^*) = -2.38 + 1.08\left(\frac{T_c}{T}\right)^2 \tag{25}$$

where T_c is the critical temperature and k^*, the Henry constant expressed in mol/L atm.

Modeling of the PSD

Theoretical considerations about the relationship between RTD and PSD

The polyolefin PSD can be influenced by parameters like the size of catalyst particles, mass and heat transfer at the particle level, particle growth, breakage, agglomeration, operating conditions, and RTD. As mentioned in "Introduction" section, PBM is often used to predict the PSD in a single CSTR. It takes into account the behavior of particle swarm, such as particle agglomeration and particle attrition. Theoretical relationships between the RTD and PSD are developed.[2,7] This methodology has the advantage of investigating the effect of the RTD on the polymer PSD. The PSD model developed in this work is also based on the RTD.

According to the references in Table I and the specific processes herein, our PSD model is based on the following assumptions:

- Based on the "reactor granule technology," the polymer particle replicates the high-generation Ziegler–Natta spherical catalyst particles. Polymer particles are spherical and have a constant density.[1] The particle porosity and polymer crystallinity are assumed constant during the particle growth.
- Particle agglomeration is absent during the polymerization. In FBRs, agglomerization may occur due to the temperature gradient in the bed and frequent particle collision.[8] However, in HSBRs, the relatively slow particle motion together with an excellent heat removal capacity may avoid particle agglomeration.[11,13]
- Particle breakage is negligible. Both the particle morphology in the early stage of the polymerization and the mechanical agitation can affect particle breakage. Unfortunately, there is a lack of study on the modeling of particle breakage in polyolefin processes.[2,12] This assumption will be discussed in Section 4.2.
- Particle residence time is independent of the particle size and is only dependent on the hydrodynamics of the reactor.

Based on the above assumptions, at the steady state, the number particle density function $N(D)$ can be related to RTD[7] by eq. (26) (see Appendix for details):

$$N(D)dD = E_{cat}(t)dt \tag{26}$$

The term $N(D)dD$ denotes the number of particles in the size range $[D, D + dD]$. Rearrangement of eq. (26) leads to $N(D)$:

$$N(D) = E_{cat}(t) \Big/ \frac{dD}{dt} \tag{27}$$

Accordingly, the probability density function $P(D)$ can be defined in terms of $N(D)$:

$$P(D) = \frac{D^3 \cdot N(D)}{\int_{D_0}^{D_{max}} D^3 \cdot N(D)dD} \tag{28}$$

$P(D)dD$ denotes the mass fraction of particles in the size range $[D, D + dD]$. Note that $P(D)$ satisfies the following normalization condition:

$$\int_{D_{\min}}^{D_{\max}} P(D)dD = 1 \tag{29}$$

Effect of the nonuniform catalyst feed

For a catalyst feed with a nonuniform PSD, the catalysts' size distribution is discretized into n intervals, each representing a mean diameter. The total PSD is superimposed according to eq. (30):

$$P(D) = \int_{D_{0,\min}}^{D_{0,\max}} P(D, D_0)P_0(D_0)dD_0 \tag{30}$$

where $P(D, D_0)$ is the PSD function for the particles of size D grown from the initial catalyst of size D_0, and $P_0(D_0)$ is the catalyst PSD function. Equation (30) can be rewritten as the following matrix:

$$\begin{bmatrix} w_1 & w_2 & w_3 & \dots & w_m \end{bmatrix} \times \begin{bmatrix} P_{11} & P_{12} & P_{13} & \cdots & & & & & \\ 0 & P_{21} & P_{22} & P_{23} & \cdots & & & & \\ 0 & 0 & P_{31} & P_{32} & P_{33} & \cdots & & & \\ \vdots & 0 & 0 & \ddots & \ddots & \ddots & \cdots & & \\ 0 & 0 & 0 & \cdots & P_{m1} & P_{m2} & P_{m3} & \cdots & P_{mn} \end{bmatrix} = \begin{bmatrix} P_{t,1} & P_{t,2} & P_{t,3} & \cdots & P_{t,m+n-1} \end{bmatrix} \tag{31}$$

where the vectors: $\boldsymbol{w} = (w_1, w_2, w_3, \dots, w_m)$ and $\boldsymbol{P}_t = (P_{t,1}, P_{t,2}, P_{t,3}, \dots, P_{t,m+n-1})$ are the catalyst mass fraction and the total polymer particle PSD, respectively. Each row of the matrix represents the polymer PSD corresponding to each catalyst interval derived from the RTD.

Methodology for the polymer PSD model

This work considers reactors R1 and R2 in Figure 1. Figure 3 shows the solution procedure for the above model. The model input includes transport properties, kinetic pre-exponential factor, activation energy, initial active catalyst concentration and diameter. The single particle growth model PMLM is used to calculate the particle growth rate. The monomer concentration and temperature profiles can also be determined from the PMLM model. Based on the particle growth rate $G(D)$ and the catalyst residence time in the reactor, eqs. (26) and are used to calculate the PSD. In the case of a nonuniform catalyst feed, eqs. (30) and (31) are performed.

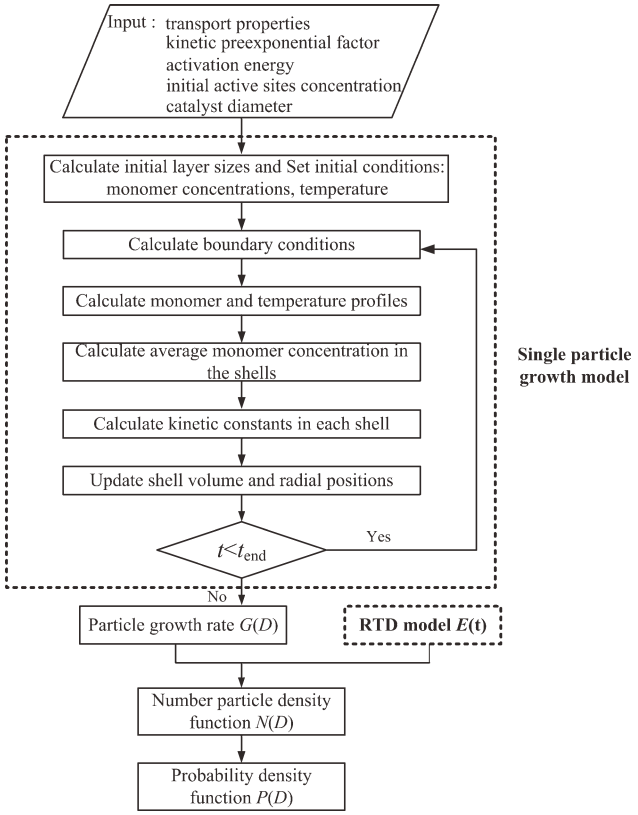

Figure 3 Methodology used to solve the PSD model.

RESULTS AND DISCUSSION

Model comparison and parametric identification

The model developed in this work is first validated by comparison with the PBM in terms of the probability density function. The population balance equation in the absence of particle agglomeration and breakage in a single CSTR can be written as eq. (32)[8]:

$$-\frac{F_1}{W}P(D) - \frac{d}{dD}[P(D)G(D)] + P(D)\frac{3}{D}G(D) = 0 \tag{32}$$

For the sake of simplicity, the activation and deactivation of the catalyst and the intraparticle mass- and heat-transfer resistances are ignored. Figure 4 shows that the two models yield very similar results. Keep in mind that the population balance equation [see eq. (32)] gives the PSD in the reactor, while the model developed in this work calculates the PSD in the outflow stream of the reactor. In the case of a CSTR, both are identical. However, in the case of a nonideal reactor, they are different. Figure 5 compares Soares's work and this one in terms of the probability density function. The agreement is good. The propagation constant and operating conditions are taken from Soares's work and are listed in the caption of Figure 5.[7] Note that the number density

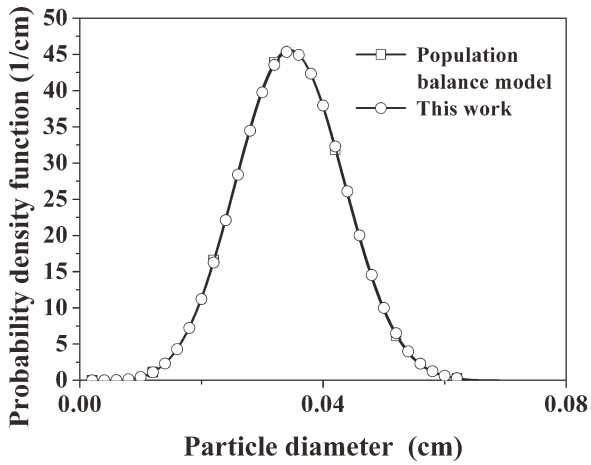

Figure 4 Comparison of polymer PSD between the results of the PBM and this work ($k_p = 1.2 \times 10^5$ L/mol min, $C_m = 4$ mol/L, $C^* = 10^{-3}$ mol/L, $k_f = 0$, $k_d = 0$, $\tau = 1.55$ h).

function obtained from Soares's work is converted to the probability density function (mass density function) so as to be consistent with our model.

According to the procedure in Figure 3, some of the parameters of the PSD model are estimated using industrial data from reactor R1. The PSD model is then used to predict the polymer PSD in reactor R2. The parameters used in the simulations are gathered in Table IV.

Comparison between experimental and simulated data

The average diameter of the initial catalyst particles is 25 μm, and its distribution is unknown. Therefore, an assumption is made that it follows a log-normal distribution[8,10]

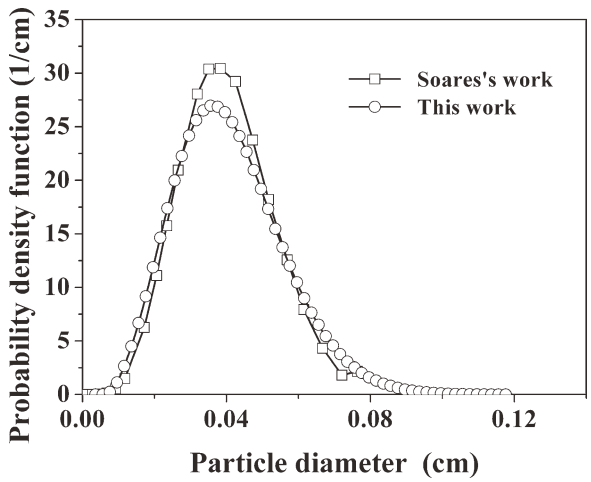

Figure 5 Comparison of polymer PSD between the model predictions and Soares's work ($k_p = 1.2 \times 10^5$ L/mol min, $C_m = 4$ mol/L, $C^* = 10^{-3}$ mol/L, $k_f = 0$, $k_d = 0$, $\tau = 2$ h).

TABLE IV
Parameters for the Simulation of the HSBR

Property	Value	Reference
Transport properties of the reaction mixture		
D_{bulk} (m^2/s)	4×10^{-7}	22
D_{eff} (m^2/s)	5.0×10^{-10}	22
μ_g (Pa s)	10^{-5}	22
u_r (m/s)	0.2	22, 23
C_{pg} (J/kg K)	1680	15
λ_g (W/m K)	0.02	22
k_e (W/m K)	0.1092	22
ΔH_r (J/mol)	1.042×10^5	22
Catalyst parameters		
d_{cat} (μm)	20–70	This work
C_0^* (mol/kg-cat)	0.035	This work
ρ_{cat} (kg/m^3)	2840	25
Polymer parameters		
ρ_{pp} (kg/m^3)	910	25
ρ_{cry} (kg/m^3)	980	25
ρ_{am} (kg/m^3)	854	25
C_p (J/kg K)	1392	22
Kinetics parameters		
E_{af} (kcal/mol)	12	15
E_{ap} (kcal/mol)	12	15
E_{ad} (kcal/mol)	12	15
k_{f0} (1/s)	4.0×10^4	This work
k_{p0} (m^3/mol s)	3.0×10^7	This work
k_{d0} (1/s)	3.7×10^3	2, 33

$$P_0(D_0) = \frac{1}{\sqrt{2\pi} D_0 \sigma} \exp\left(-\frac{\left(\ln D_0 - \ln \overline{D}_0\right)^2}{2\sigma^2} \right) \quad (33)$$

The standard deviation σ is chosen as an adjustable parameter. The flow Model 1 is used to describe the HSBR. Figure 6 compares the fitted polymer PSD with the one obtained experimentally from reactor R1. The agreement is good except for particles smaller than 0.04 cm in diameter. This reveals that the polymer particles in the industrial reactor R1 have more fine particles (<0.04 cm). As stated in the model assumptions (the fourth item), this can be

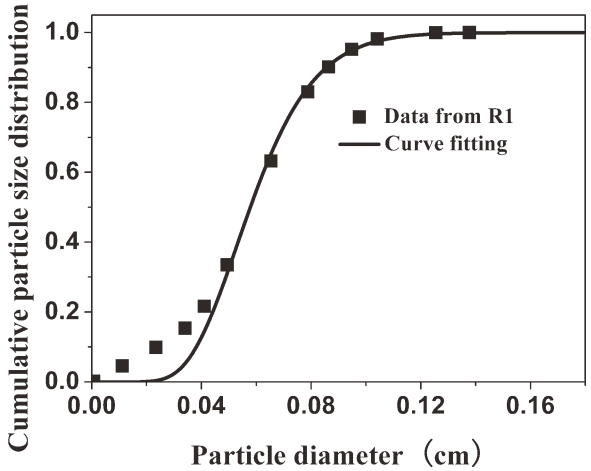

Figure 6 Polymer PSD from reactor R1.

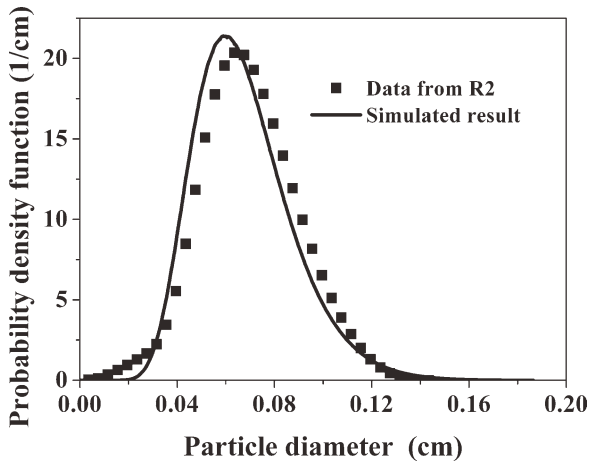

Figure 7 Comparison of the polymer PSD between the simulation and the industrial data from reactor R2.

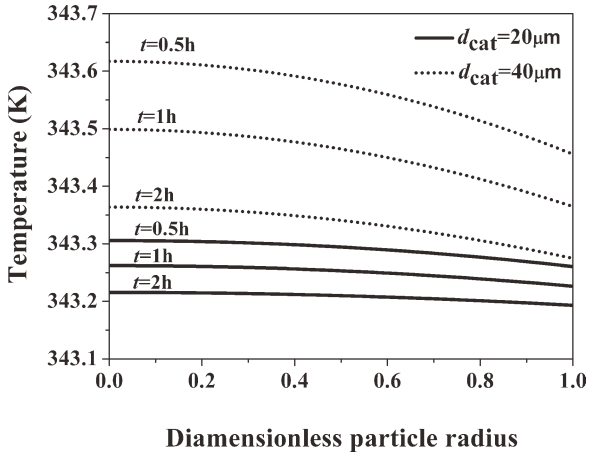

Figure 9 Spatial temperature profiles for two different catalyst sizes at three different times.

interpreted by two aspects: first, the mechanical agitation ensured by the paddles may break up some of the growing polymer particles; second, the polymer particle can undergo fast fragmentation into fine powder because of the absence of the prepolymerization step in this process.

Once the model parameters are obtained from reactor R1, the model can be used to predict the polymer PSD in the outflow streams of reactor R2. Figure 7 shows that the predicted PSD agrees well with the industrial one, confirming the validity of the PSD model developed in this work.

Simulation of PSD in HSBRs

Effects of the catalyst particle size

Figure 8 shows the time evolution of the propylene concentration profiles in the catalyst particle as a function of the dimensionless particle radius. As the initial catalyst size increases, the propylene concentration in the particle decreases because of mass-transfer limitations. As a result, large radial concentration gradients can arise inside the catalyst/polymer particle during the early stages of polymerization. The results also reveal that the time required for eliminating the propylene concentration radial gradients in the particle increases, as the initial catalyst size increases. On the other hand, according to the results of Figure 9, no significant radial temperature gradients arise inside the catalyst/polymer particle, even at earlier polymerization times.

In the simulations, the catalyst concentration of active sites is kept constant, that is, $C^*_0 = 3.5 \times 10^{-2}$ mol/kg-cat. This means that the total molar mass of the active sites increases with increasing initial catalyst size. From Figure 10, although large radial concentration gradients may arise inside the catalyst/polymer particle at early stages of polymerization for a larger catalyst size, the particle growth rate increases, as the initial catalyst size increases because of a higher amount of active sites. Consequently, the polymer PSD becomes broader with

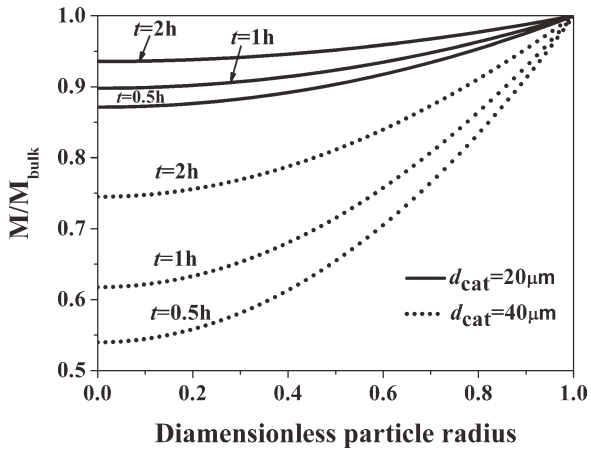

Figure 8 Spatial propylene concentration profiles for two different catalyst sizes at three different times.

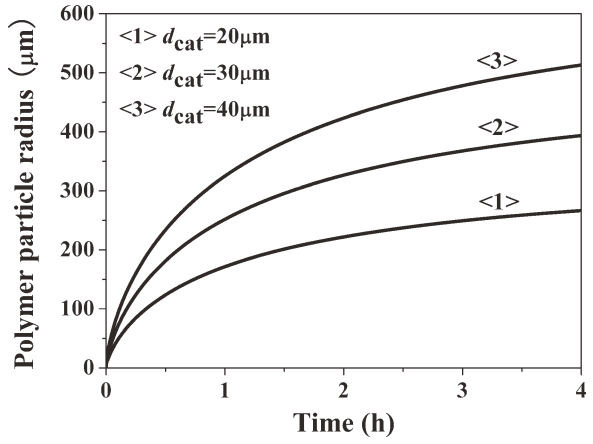

Figure 10 Polymer particle growth rates with three different catalyst sizes.

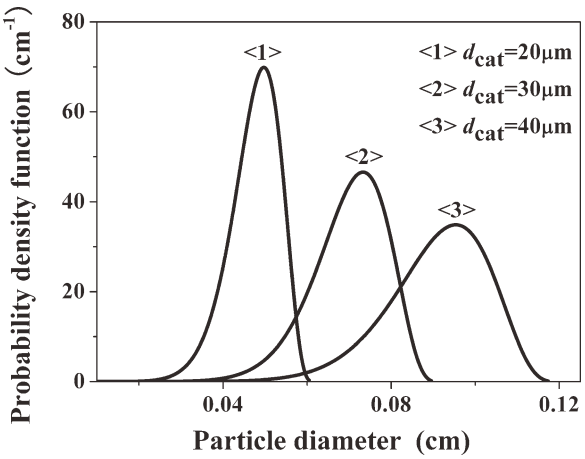

Figure 11 Effect of the catalyst size on the polymer PSD in reactor R1.

increasing catalyst size in R1 with a concomitant shift of the PSD to larger particles (see Figure 11).

One of the most important transport properties for calculating the growth rate of a catalyst/polymer particle in gas-phase olefin polymerization is the effective monomer diffusion coefficient. Figure 12 shows the influence of the effective monomer diffusion coefficient on the polymer PSD. The latter is shifted to larger particles with an increase in D_{eff}. However, the polymer PSD changes slightly, when the value of D_{eff} is 5×10^{-10} m^2/s. This could be explained by the propylene concentration profiles inside the particle (see Figure 13). Large concentration gradients arise inside the catalyst/polymer particle with decreasing D_{eff}. When the value of D_{eff} is as low as 10^{-11} m^2/s, the rate of the monomer transfer from the bulk gas phase to the active catalyst sites becomes the limiting step in the polymerization,. In contrast, when the value of D_{eff} is close to

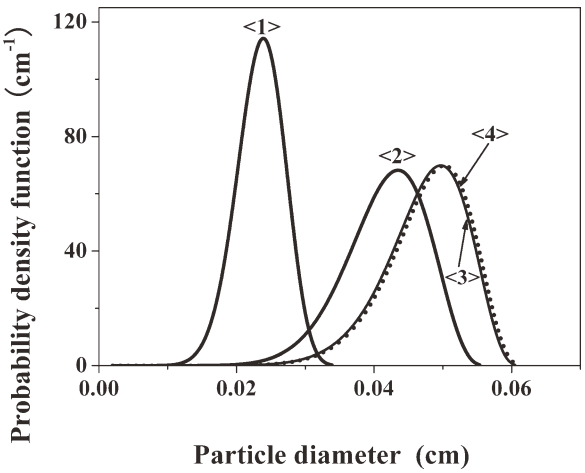

Figure 12 Effect of the effective monomer diffusion coefficient on the polymer PSD in R1 ($\langle 1 \rangle$ $D_{eff} = 10^{-11}$ m^2/s; $\langle 2 \rangle$ $D_{eff} = 5 \times 10^{-11}$ m^2/s; $\langle 3 \rangle$ $D_{eff} = 5 \times 10^{-10}$ m^2/s; $\langle 4 \rangle$ $D_{eff} = 5 \times 10^{-9}$ m^2/s, $d_{cat} = 20$ μm).

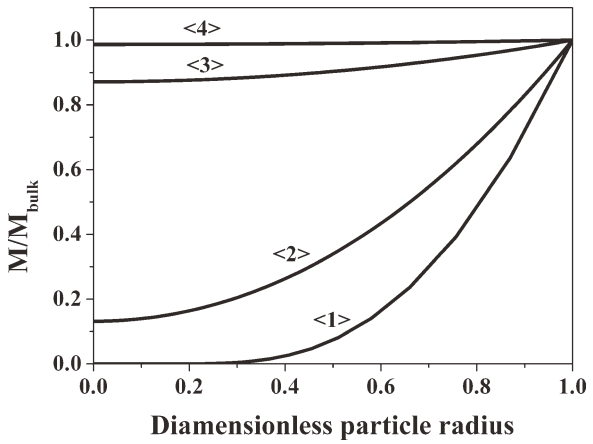

Figure 13 Effect of the effective monomer diffusion coefficient on the propylene concentration profiles at $t = 0.5$ h ($\langle 1 \rangle$ $D_{eff} = 10^{-11}$ m^2/s; $\langle 2 \rangle$ $D_{eff} = 5 \times 10^{-11}$ m^2/s; $\langle 3 \rangle$ $D_{eff} = 5 \times 10^{-10}$ m^2/s; $\langle 4 \rangle$ $D_{eff} = 5 \times 10^{-9}$ m^2/s, $d_{cat} = 20$ μm).

5×10^{-10} m^2/s, no remarkable monomer concentration gradients arise inside the particle, and the intrinsic kinetics dominates the rate of polymerization.

Figure 14 shows the effect of the polymer crystallinity on the polymer PSD. The shift of the PSD curve to small particles is due to a decrease in the amount of the sorbed monomer in the amorphous polymer phase. It is well known that the propylene solubility and permeability in the polymerization system is dependent on the polymer crystallinity. In fact, the effective monomer diffusion coefficient decreases with increasing polymer crystallinity.[25] As pointed out in the previous paragraph, a decrease in D_{eff} can also result in smaller polymer particles.

Effect of the RTD

Based on Dittrich's work,[11] Models 1–3 are used to describe the flow in reactor R2. The reason for

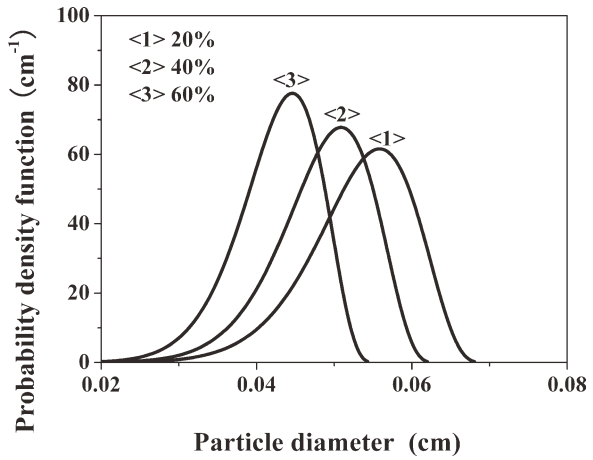

Figure 14 Effect of the polymer crystallinity on the polymer PSD in R1 ($D_{eff} = 5 \times 10^{-10}$ m^2/s, $d_{cat} = 20$ μm).

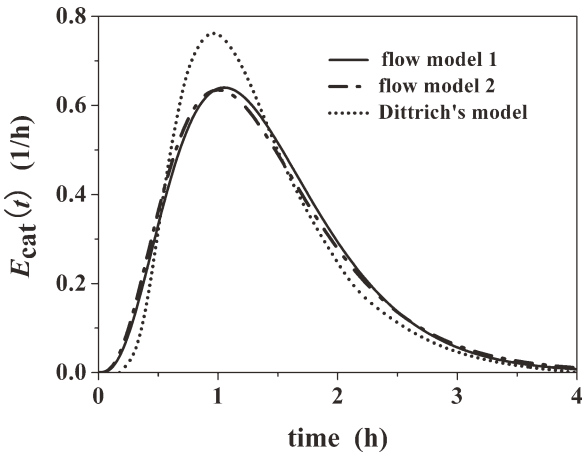

Figure 15 RTDs predicted by three different flow models.

choosing reactor R2 is that its average residence time is 1.4 h, which is close to Dittrich's RTD data. Figure 15 shows the RTDs in reactor R2 predicted by the above three models. Those predicted by Models 1 and 2 are close to each other, and they are significantly wider than the one predicted by Model 3 (Dittrich's model). The following sections will show that the different RTDs may have different influence on the simulated polymer PSD results.

Figure 16 shows the polymer PSDs predicted by the three models for a uniform size catalyst feed. The average polymer particle diameter predicted by the RTD of Model 3 is 490 μm, which is slightly smaller than those of Models 1 (510 μm) and 2 (510 μm). For a nonuniform size catalyst feed, the PSDs of the three models are almost the same (see Figure 17). This is in agreement with Dittrich's work (2007) and could be explained by the fact that both the catalysts PSD and RTD affect the polymer PSD but in a different manner. As a result, the effect of the RTD on the polymer PSD is less obvious for a nonuniform size catalyst feed than for a uniform one.

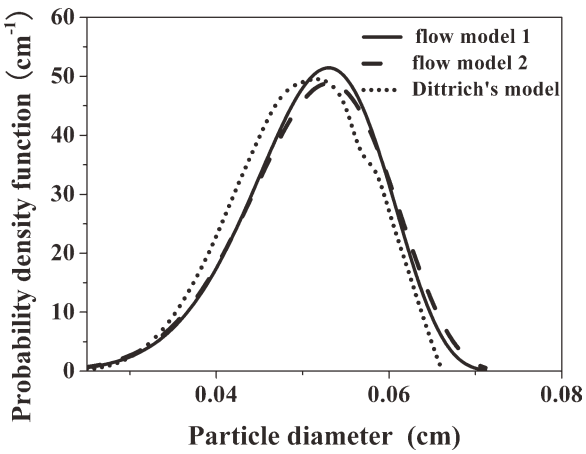

Figure 16 Comparison of the polymer PSD among three different flow models for a uniform size catalyst feed.

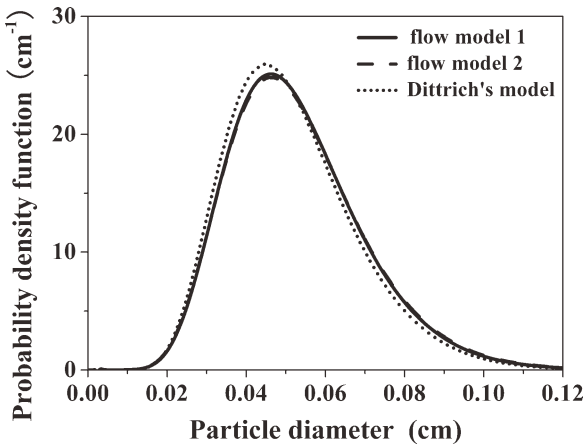

Figure 17 Comparison of the polymer PSD among three different flow models for a nonuniform size catalyst feed.

CONCLUSIONS

A steady-state PSD model is developed to predict the size distribution of polypropylene particles in the outflow streams of industrial HSBRs. The PMLM is used to calculate the growth rate of a single particle under the internal and external heat and mass transfer limitations. The model takes into account both the single polymer particle growth and the catalyst RTD. It is validated by data generated from industrial processes at steady state. The polymer PSDs predicted by the model agree satisfactorily with the industrial data.

The effects of the internal mass and heat transfer limitations on the particle growth, the intraparticle monomer, and temperature profiles are predicted by the PMLM. The results reveal that the effect of the intraparticle mass resistance is important, and no remarkable temperature gradients inside the particle are observed for the propylene polymerization in the HSBRs. The effects of the feed catalyst particle size,

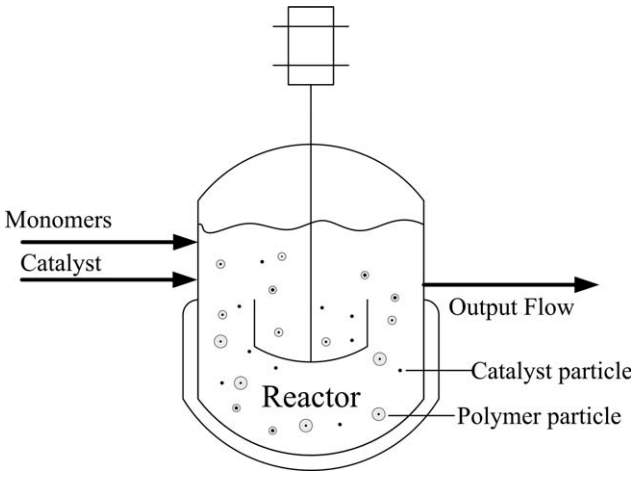

Figure 18 Schematic diagram of a continuous olefin polymerization process.

the internal mass transfer resistance, and polymer crystallinity on the polymer PSD in the HSBRs are also investigated in this work. The internal mass transfer resistance and the initial catalyst size greatly affect the polymer PSD. An increase in the polymer crystallinity shifts the PSD to a smaller particle size.

The effect of the catalyst RTD on the polymer PSD is also simulated by the model. In the case of a non-uniform size catalyst feed, the PSDs predicted from three different flow models are not very different from each other. The reason is that both the catalysts PSD and RTD affect the polymer PSD and their effects oppose each other.

NOMENCLATURE

a_φ volume fraction of the amorphous phase in polymer (1)
C_m actual concentration of monomer absorbed in the polymer (kg m^{-3})
C^j_{mi} actual concentration of monomer absorbed in layer i at the jth time interval (kg m^{-3})
C_{pg} heat capacity of the gas phase (J kg^{-1} K^{-1})
C_p heat capacity of the polymer particle (J kg^{-1} K^{-1})
C^*_0 initial number of active sites per kilogram of catalysts (mol kg-cat^{-1})
C^* number of active sites per kilogram of catalysts (mol kg-cat^{-1})
C^{*j}_i concentration of active sites based on volume of layer in layer i at jth time interval (mol m^{-3})
D polypropylene particle diameter (m)
D_{bulk} monomer diffusion coefficient in bulk phase (m^2 s^{-1})
D_{eff} effective monomer diffusion coefficient in polymer phase (m^2 s^{-1})
d_{cat} catalyst diameter (m)
d_p particle diameter (m)
$E(t)$ RTD density function (s^{-1})
E_{af} activation energy for the lumped activation reactions (kcal mol^{-1})
E_{ap} activation energy for the lumped propagation reactions (kcal mol^{-1})
E_{ad} activation energy for the lumped deactivation reactions (kcal mol^{-1})
F_1 flow rate of the outflow streams of polymer particles (kg s^{-1})
$G(D)$ particle growth rate (m s^{-1})
ΔH_r heat of polymerization (J mol^{-1})
H external film heat transfer coefficient (W m^{-2} K^{-1})
h_m external film mass transfer coefficient (m s^{-1})
k_d deactivation constant (s^{-1})
k_{d0} frequency factor (s^{-1})
k_e thermal conductivity (W m^{-1} K^{-1})
k_f activation constant (s^{-1})
k_{f0} frequency factor (s^{-1})
k_p propagation rate constant (m^3 $mol^{-1}s^{-1}$)
k_{p0} frequency factor (m^3 $mol^{-1}s^{-1}$)
k^* Henry constant (mol L^{-1} atm^{-1})
M monomer concentration in polymer particle (mol m^{-3})
M_{bulk} monomer concentration of bulk phase (mol m^{-3})
$[M]^*$ moles of monomer per unit volume amorphous polymer (mol m^{-3}-amor)
$N(D)$ number density function (m^{-1})
N_{CSTR} number of tanks (1)
Nu Nusselt number (1)
P pressure (bar)
$P(D)$ mass density function (m^{-1})
P_m the monomer pressure inside polymer particle (atm)
P_{mn} the value of polymer PSD produced by the catalyst at the mth intervals (m^{-1})
Pr Prandtl number (1)
P_t total polymer PSD (m^{-1})
R radius of polymer particle (m)
Re Reynolds (1)
R_{gas} gas constant (J mol^{-1} K^{-1})
R_M monomer consumption rate (mol m^{-3} s^{-1})
R_p polymerization rate (mol kg-$cat^{-1}s^{-1}$)
R radial position in growing polymer particle (m)
r^j_i radial position of the layer i at the jth time interval (m)
Sc Scmidt number (1)
Sh Sherwood number (1)
S_p potential active sites per kilogram of catalyst (mol kg-cat^{-1})
T temperature (K)
T_{bulk} bulk phase temperature (K)
T_c the critical temperature (K)
t residence time (s)
u_r particle-fluid relative velocity (m s^{-1})
V^j_i the volume of layer i at the jth time interval (m^3)
W catalyst weight fraction (1)

Greek symbols

λ_g thermal conductivity of gas phase (W m^{-1} K^{-1})
μ_g viscosity of gas phase (Pa s)
ρ_a density of amorphous polymer (kg m^{-3})
ρ_{cat} catalyst density (kg m^{-3})
ρ_c density of crystalline polymer (kg m^{-3})
ρ_p polypropylene density (kg m^{-3})
σ standard deviation (1)
τ mean residence time (s)

APPENDIX

Figure 18 shows polymer particles in a continuous olefin polymerization. To derive eq. (12), a population balance for polymer particles is performed. Based on the assumptions for the model, one has:

$$\text{Number of polymer particles} = \text{Number of catalyst particles} \quad \text{(A1)}$$

The catalyst mass fraction of exit stream of age between t and $t + dt$ is

$$E_{\text{cat}}(t)dt \quad \text{(A2)}$$

For a uniform catalyst-size distribution, eq. (A2) also represents the catalyst number fraction of exit stream of age between t and $t + dt$. The size of a single polymer particle is dependent on the residence time of the initial corresponding catalyst particle. From eqs. (A1) and (A2), one can write:

$$\text{Catalyst number fraction of exit stream of age between t and } t + dt = \text{Polymer number fraction of exit stream of volume between } V \text{ and } V + dV \quad \text{(A3)}$$

As it is assumed that polymer particles are spherical and have constant density, eq. (A3) becomes

$$E_{\text{cat}}(t)dt = N(D)dD \quad \text{(A4)}$$

where $N(D)dD$ represents the number fraction of polymer particles whose diameter ranges from D to $D + dD$.

References

1. Galli, P.; Vecellio, G. Prog Polym Sci 2001, 26, 1287.
2. Zacca, J. J.; Debling, J. A.; Ray, W. H. Chem Eng Sci 1996, 51, 4859.
3. Harshe, Y. M.; Utilar, R. P.; Ranade, V. V. Chem Eng Sci 2004, 59, 5145.
4. Dompazis, G.; Kanellopoulos, V.; Touloupides, V.; Kiparissides, C. Chem Eng Sci 2008, 63, 4735.
5. Urdampilleta, I.; Gonza'lez, A.; Iruin, J. J.; de la Cal, J. C.; Asua, J. M. Ind Eng Chem Res 2006, 45, 4178.
6. Choi, K. Y.; Zhao, X.; Tang, S. H. J Appl Polym Sci 1994, 53, 1589.
7. Soares, J. B. P.; Hamielec, A. E. Macromol Theory Simul 1995, 4, 1085.
8. Hatzantonis, H.; Goulas, A.; Kiparissides, C. Chem Eng Sci 1998, 53, 3251.
9. Yiannoulakis, H.; Yiagopoulos, A.; Kiparissides, C. Chem Eng Sci 2001, 56, 917.
10. Kim, K. Y.; Choi, K. Y. Chem Eng Sci 2001, 56, 4069.
11. Dittrich, C. J.; Mutsers, A. M. P. Chem Eng Sci 2007, 62, 5777.
12. Luo, Z. H.; Su, P. L.; You, X. Z.; Shi, D. P.; Wu, J. C. Chem Eng J 2009, 146, 466.
13. Caracotsios, D. M. Chem Eng Sci 1992, 47, 2591.
14. Mattos Neto, A. G.; Pinto, J. C. Chem Eng Sci 2001, 56, 4043.
15. Gorbach, A. B.; Naik, S. D.; Ray, W. H. Chem Eng Sci 2000, 55, 4461.
16. Khare, N. P.; Lucas, B.; Seavey, K. C.; Liu, Y. A. Ind Eng Chem Res 2004, 43, 884.
17. Chen, L. Q.; Hu, G. H. AIChE J 1993, 39, 1558.
18. Yong, W. Y.; Cao, W. W.; Chung, T. C.; Morris, J. Applied Numerical Methods using MATLAB; Wiley: Hoboken, New Jersey, 2005.
19. Soares, J. B. P.; Hamielec, A. E. Polym React Eng 1995, 3, 261.
20. Sun, J. Z.; Eberstein, C.; Reichert, K. H. J Appl Polym Sci 1997, 64, 203.
21. Luo, Z. H.; Wen, S. H.; Shi, D. P.; Zheng, Z. W. Macromol React Eng 2010, 4, 123.
22. Floyd, S.; Choi, K. Y.; Taylor, T. W.; Ray, W. H. J Appl Polym Sci 1986, 32, 2935.
23. Floyd, S.; Choi, K. Y.; Taylor, T. W.; Ray, W. H. J Appl Polym Sci 1986, 31, 2231.
24. Kosek, J.; Grof, Z.; Novák, A.; Štepánek, F.; Marek, M. Chem Eng Sci 2001, 56, 3951.
25. Kanellopoulos, V.; Dompazis, G.; Gustafsson, B.; Kiparissides, C. Ind Eng Chem Res 2004, 43, 5166.
26. Samson, J. J. C.; Weickert, G.; Heerze, A. E.; Westerterp, K. R. AIChE J 1998, 44, 1424.
27. Samson, J. J. C.; Middelkoop, B. V.; Weickert, G.; Westerterp, K. R. AIChE J 1999, 45, 1548.
28. Pater, J. T. M.; Weickert, G.; Loos, J.; van Swaaij, W. P. M. Chem Eng Sci 2001, 56, 4107.
29. Pater, J. T. M.; Weickert, G.; van Swaaij, W. P. M. Chem Eng Sci 2002, 57, 3461.
30. Kissin, Y. V. Alkene Polymerization Reactions with Metal Catalysts; Elsevier: Amsterdam, 2008.
31. Hutchinson, R. A.; Ray, W. H. J Appl Polym Sci 1990, 41, 51.
32. Stern, S. A.; Mullhaupt, J. T.; Gareis, P. J. AIChE J 1969, 15, 64.
33. Zacca, J. J.; Debling, J. A.; Ray, W. H. Chem Eng Sci 1997, 52, 1941.